

Quantification of Boundary Layer Mixing over the Southern Ocean Using In-Situ and Remotely-Sensed Measurements

Sean Hartery^{1,1}, Peter Kuma^{1,1}, Mike J Harvey^{2,2}, and Adrian J. McDonald^{1,1}

¹University of Canterbury

²NIWA

November 30, 2022

Abstract

We demonstrate that the relationship between the abundance of particulate surface area observed at sea-level and measurements of backscattered light by a ceilometer can be used to classify the mixing state of the atmospheric layer beneath the lowest observed cloud, where the relationship is defined by the Spearman Rank correlation. The accuracy of this correlation-based method was compared to two methods of detecting boundary layer decoupling based on radiosonde measurements. An optimized version of the new methodology correctly determined the mixing state of the below-cloud layer for $76 \pm 4\%$ of the radiosondes available for comparison. Further, it was more accurate than an alternative ground-based metric used to determine the below-cloud mixing state. For the majority of the time series in which the correlation analysis could be applied, the below-cloud boundary layer was well-mixed (54%), or else fog was present (27%), which indicated that aerosol particles observed at sea-level often have a direct pathway into low-cloud (81%). In the remaining analysis period, the near-surface atmospheric layer was stable and the atmospheric layer near the ocean surface was decoupled from the overlying cloud (19%). Forecasts from the Antarctic Mesoscale Prediction System also support our findings, showing that conditions that mix aerosol particles from the ocean surface to the lowest observed cloud occur 84% of the time over the open Southern Ocean. As a result, aerosol particles measured near sea-level are often tightly coupled to low-cloud formation over the Southern Ocean, highlighting the utility of shipborne aerosol observations in the region.

Classification of the Below-Cloud Mixing State Over the Southern Ocean Using In-Situ and Remotely-Sensed Measurements

S. Hartery¹, P. Kuma¹, M.J. Harvey², and A.J. McDonald¹

¹School of Physical and Chemical Sciences, University of Canterbury, Christchurch, New Zealand

²National Institute of Water and Atmospheric Research, Wellington, New Zealand

Key Points:

- A new, correlation-based method determines the mixing state of the below-cloud layer with an accuracy of 76%.
- The below-cloud layer is only ever poorly-mixed when winds are below 8 m s⁻¹ and the near-surface atmosphere is neutrally stable.
- Sea spray particles are available to low-level cloud over the Southern Ocean more than 80% of the time throughout austral summer.

Corresponding author: Hartery, S., hartery.s.p@gmail.com

Abstract

We demonstrate that the relationship between the abundance of particulate surface area observed at sea-level and measurements of backscattered light by a ceilometer can be used to classify the mixing state of the atmospheric layer beneath the lowest observed cloud, where the relationship is defined by the Spearman Rank correlation. The accuracy of this correlation-based method was compared to two methods of detecting boundary layer decoupling based on radiosonde measurements. An optimized version of the new methodology correctly determined the mixing state of the below-cloud layer for $76 \pm 4\%$ of the radiosondes available for comparison. Further, it was more accurate than an alternative ground-based metric used to determine the below-cloud mixing state. For the majority of the time series in which the correlation analysis could be applied, the below-cloud boundary layer was well-mixed (54%), or else fog was present (27%), which indicated that aerosol particles observed at sea-level often have a direct pathway into low-cloud (81%). In the remaining analysis period, the near-surface atmospheric layer was stable and the atmospheric layer near the ocean surface was decoupled from the overlying cloud (19%). Forecasts from the Antarctic Mesoscale Prediction System also support our findings, showing that conditions that mix aerosol particles from the ocean surface to the lowest observed cloud occur 84% of the time over the open Southern Ocean. As a result, aerosol particles measured near sea-level are often tightly coupled to low-cloud formation over the Southern Ocean, highlighting the utility of shipborne aerosol observations in the region.

Plain Language Summary

Particles suspended in the atmosphere (aerosol) act as seeds for cloud droplet formation. The abundance of such particles directly influences the opacity of clouds, while their physical and chemical characteristics govern if and when those cloud droplets freeze. As a result, both the amount of solar radiation a cloud can reflect and the temperature of waters below are sensitive to the quantity and type of particles available to the cloud. We present a new methodology for understanding the conditions in which low-level clouds have direct access to the large and diverse reservoir of particles in the surface layer. We find that meteorological conditions which transfer particles from sea-level to low-level cloud are satisfied up to 81% of the time over the Southern Ocean. This suggests that the particles we observe near the surface almost always play a significant role in the formation of low-level cloud.

1 Introduction

The balance of incoming and outgoing shortwave radiation is mediated by the presence of clouds, and to a lesser extent, aerosol particles. While aerosol particles are significantly smaller than clouds, they are the seeds of cloud droplet formation (Pruppacher et al., 1998). The chemical and physical nature of these particles strongly determines both the ultimate phase of cloud droplets (e.g. liquid or ice) and the resulting size distribution of cloud droplets (Twomey, 1977). It therefore follows that errors in how these particles are represented within global climate models can cause significant climatological biases in the radiative balance. In particular, it has been observed that uncertainties in predicting cloud phase leads to substantial biases in the radiation balance within the cold sector of Southern Ocean cyclones (Bodas-Salcedo et al., 2014). While the abundant cyclones of the Southern Ocean occur solely as a function of favourable synoptic conditions (Irving et al., 2010), a global climate model’s predictions of cloud phase in the cold sector of Southern Ocean cyclones (Vergara-Temprado et al., 2018), and in the wider Southern Ocean (Schuddeboom et al., 2019), is extremely sensitive to the properties of

particles in the underlying boundary layer. In addition, recent observations directly show that the large biases between modeled and observed outgoing shortwave radiation (Trenberth & Fasullo, 2010) are related to errors in how low-level cloud are represented within global climate models (Kuma et al., 2020). Improving our understanding of the conditions in which particles can reach, and form, low-level cloud is therefore crucial to understanding the radiation balance over the Southern Ocean.

As wind speeds have increased over the Southern Ocean (Young et al., 2011; Hande et al., 2012a), there is significant interest in how naturally-produced particles impact cloud formation and the optical properties of the resultant clouds (McCoy et al., 2015), and whether this interaction represents a substantial climate feedback (Korhonen et al., 2010). It is well-known that increasing the population of cloud condensation nuclei (CCN) directly increases the opacity of the overlying cloud (Twomey, 1977). Increases in wind speed over the open ocean will enhance the flux of sea spray particles (SSPs) from breaking waves (Hartery et al., 2020). In most regions of the Southern Ocean SSPs are the only local source of ice-nucleating particles (INPs) (DeMott et al., 2016), a region almost entirely devoid of such particles (Bigg & Hopwood, 1963). While other, more potent, INPs like dust particles may be entrained into the boundary layer in specific seas (e.g. coastal seas near Patagonia), ice nucleating particles collected on Southern Ocean voyages have a much weaker surface activity than dust particles, which reflects the predominant abundance of sea spray (McCluskey et al., 2018). These particles can have a substantial influence on the radiative and physical properties of the resulting cloud. Not only are ice clouds much less opaque (Hu et al., 2010), they are much more likely to precipitate (Borys et al., 2003). Thus, changes in the abundance of SSPs may have significant impacts on cloud radiative properties.

One of the challenges in unravelling aerosol–cloud interactions over the Southern Ocean is that the region is frequently covered in cloud (80% of the time; Haynes et al. (2011)), which leads to difficulties in monitoring low-level clouds (McErlich et al., 2021) and the structure of boundary layer below (Hande et al., 2015). While in situ observational records of radiosondes from Macquarie Island provide rich data on the thermodynamic structure of the Southern Ocean boundary layer (Hande et al., 2012b), a lack of accompanying observations of CCN, INPs, and in situ microphysical properties of low-level cloud leaves a gap in our understanding of how these particles interact with cloud over the Southern Ocean. Previous research, such as the dedicated ACE-1 (Russell et al., 1998), SOCEX (Boers et al., 1998), HIPPO (Wofsy, 2011) and more recently SOCRATES (McFarquhar et al., 2020) campaigns have used aircraft observations to bridge this knowledge gap. However, aircraft can only fly in a limited range of conditions, as the strong vertical wind shear and icing conditions present within boundary layer cloud poses a significant threat. By contrast, ship-based measurements can be made in nearly all conditions. Here, we use measurements on the R/V *Tangaroa* during a voyage to the Ross Sea in the austral summer of 2018 to establish conditions in which particles near the surface are turbulently mixed to cloud base (Kremser et al., 2020). Establishing conditions when sea-level measurements are relevant to cloud will enable future research to better exploit sea-level measurements in aerosol–cloud interaction studies, and adds value to the growing catalogue of near-surface measurements available from recent voyages.

2 Measurements

Over the course of a voyage between New Zealand and the Ross Sea, air was drawn from the mast of the R/V *Tangaroa* (~20 m above sea level “a.s.l.”) to a shipping container laboratory (~2 m a.s.l.) via 40 m of conductive hose. Within the laboratory, a passive cavity aerosol spectrometer probe (PCASP-100X; Droplet Measurement Technologies) and a differential mobility particle sizer (DMPS, TSI) mea-

sured the ambient concentration of particles suspended in the atmosphere (Kremser et al., 2020). The PCASP measured the number concentration size spectra of particles suspended in the boundary layer in 30 size bins ($0.1\text{--}3.0\ \mu\text{m}$) every minute. The DMPS measured the number concentration size spectra in the size range $0.02\text{--}0.3\ \mu\text{m}$ every 10 minutes. Following Modini et al. (2015) and Quinn et al. (2017), we fit three lognormal size distributions to estimate the average diameter and number concentration of Aitken, accumulation and coarse mode particulate. With rare exception, coarse mode particulate is almost entirely composed of sea spray particles (SSPs) in the marine environment (Modini et al., 2015; Quinn et al., 2017); hence, we will refer to the coarse mode as the SSP mode throughout the remainder of this work. The PCASP was used exclusively to estimate the average size and abundance of SSPs, while the DMPS was used for the Aitken and accumulation mode particles. When data from the DMPS were not available, measurements from the PCASP were used to constrain the abundance and size of accumulation mode particles. Further details on sampling set-up and analysis, including correction factors for losses through the sampling line and methods for handling contamination from ship exhaust, are described in Hartery et al. (2020) and Kremser et al. (2020). In parallel to the size-resolved particle concentration spectra generated by the SMPS and PCASP, the total number of cloud condensation nuclei (CCN) was measured using a CCN counter (CCNC-100; Droplet Measurement Technologies). The CCN counter sampled from the same sampling conduit that drew ambient air to the PCASP and DMPS. A measurement of the average number of ambient CCN was made twice an hour at intervals of 0.1% supersaturation between 0.2–1.0%.

A ceilometer (CHM-15K; Lufft) transmitted pulses of laser light at a wavelength of 1064 nm and recorded the total power of light scattered back to the ceilometer per laser pulse from different levels of the atmosphere. Measurements were recorded at a temporal resolution of one record per minute and a vertical resolution of 15 m. For each record, the instrument also estimated the cloud base height, z_{CBH} . A raw quality control flag provided by the instrument was used to screen for field-of-view contamination from fog or residual precipitation on the outer optical window. A micro-rain radar (MRR-2; Metek) operated in proximity was also used to detect and screen for precipitation events.

An Automated Weather Station (AWS) provided by New Zealand MetService was positioned above the bridge of the R/V *Tangaroa* at 22.5 m. Relevant measurements included ambient pressure, air temperature, relative humidity, long and shortwave radiation fluxes, wind speed, and wind direction. Measurements from the AWS were corrected to a height of 10 m according to the COARE 3.5 bulk-flux algorithms (Edson et al., 2013) as detailed in Hartery et al. (2020). The bulk seawater temperature was measured at a depth of 5.5 m below sea level with a thermistor (SBE38; Sea-Bird Scientific). We also used the COARE 3.5 bulk-flux algorithms (Edson et al., 2013) to calculate the sea skin temperature from the bulk temperature, accounting for long and shortwave fluxes (Edson et al., 2013).

Fifty-seven meteorological balloons were launched during the voyage. The radiosondes (iMet-ABx; InterMet) recorded pressure, relative humidity, temperature and wind speed. In quality control, two of the radiosondes were found to have a faulty relative humidity sensor and one had more than one faulty sensor, leaving 54 useful profiles of the boundary layer. The radiosondes were launched approximately twice daily once the ship was further south than 60°S .

Regional meteorological forecasts were downloaded from the Antarctic Mesoscale Prediction System (AMPS). AMPS initializes a new forecast every twelve hours, with subsequent output provided every three hours. AMPS provides forecasts within several nested spatial grids. However, only forecasts for the outermost spatial grid, “domain 1,” were used as it was the only grid which fully contained the

ship track. Domain 1 has a horizontal resolution of 24 km and is a 544×412 grid centred on 90°S. AMPS uses the Mellor-Yamada-Janjić (MYJ) scheme, a 2.5-level closure model of turbulence, to predict the behavior of the planetary boundary layer (PBL). AMPS calculates the height of the PBL to be the height at which the turbulent kinetic energy falls below a pre-determined threshold (Janjić, 2001). To allow for a brief model spin-up, only forecasts between 3–12 hours were used (Jolly et al., 2016).

3 Methods

3.1 Classification of the Below-Cloud Layer

The suspended particle cross-sectional surface area, A , was calculated from the number concentration size spectra measured by the PCASP:

$$A(t) = \int \frac{dn(t, D_p)}{d \log D_p} \pi \left(\frac{D_p}{2} \right)^2 d \log D_p \quad (1)$$

Where D_p is the particle diameter, n is the partial concentration of particles, and t is time. Note that as this is a correlation-based study, a more exact treatment of the interaction of particulate with light which accounts for both Mie and Rayleigh scattering (e.g. Bohren and Huffman (1983)) is not strictly necessary. In addition, such calculations would necessitate *a priori* information about particle composition and morphology which were not available for this study. The geometric surface area is dominated by the sea spray and accumulation mode particles (97%, on average; Fig. 1d), which the PCASP can readily measure.

To classify the below-cloud layer mixing state, we calculated rolling Spearman Rank correlation coefficients centred on each hour of observation between the sea-level concentration of aerosol surface area, $A(t)$, and the background-corrected total power of backscattered light received by the ceilometer, P_c . The Spearman Rank correlation coefficient was used as non-linearities related to the two-way transmission of light through an atmospheric layer are likely; however, the Pearson moment correlation coefficient produced qualitatively similar results. Before calculating the correlation coefficients, four quality control measures were implemented to ensure that the calculated correlation coefficients would be meaningful. First, the observations were screened based on the ceilometer’s quality control flag and the ship contamination flag described in Kremser et al. (2020). Second, only backscattered light retrieved from heights below the 10th-percentile of CBH were studied. This step ensured that correlations between backscattered light from a given altitude and sea-level particulate surface area resulted from co-variations of the abundance of aerosol particles at the surface and the selected height and not from variations in the presence of cloud droplets. Next, we performed a signal-to-noise analysis, where the signal-to-noise ratio (SNR) is defined as follows:

$$\text{SNR} = \frac{P(t, z)}{P_{bg}(t)} \quad (2)$$

P_{bg} is the ceilometer’s background signal, which the instrument measures at the end of its laser pulse cycle, P is the raw laser power received by the instrument and z is the altitude a.s.l. from which the backscattered light was retrieved. We removed any data points from profiles which had an SNR less than two. Following the SNR analysis, the total power of backscattered light detected by the ceilometer, $P(t, z)$, was corrected for the background signal:

$$P_c(t, z) = P(t, z) - P_{bg}(t) \quad (3)$$

Following the initial quality control, rolling correlation coefficients were calculated between $A(t)$ and $P_c(t, z)$. This was completed in a two-step process. First, a sub-set

of the time-series, T , was defined:

$$T = \{t_{i-\Delta t/2}, t_{i-\Delta t/2+1}, \dots, t_{i+\Delta t/2}\} \quad (4)$$

where t_i is a specific time in the observation period and Δt defines the temporal width of the sub-set around t_i . In this work, temporal widths between 1 and 20 hours were studied. As observations were recorded every minute, the sub-set T contained at least 60 data points and at most 1200. Spearman Rank Correlation coefficients, r_s , were then calculated as follows:

$$r_s(x, y) = \frac{\text{cov}(\text{rank}(x), \text{rank}(y))}{\sigma_{\text{rank}(x)} \sigma_{\text{rank}(y)}} \quad (5)$$

where $\text{rank}(x)$ is a function which assigns an integer ranking to each value of a set x ; $\text{cov}(x, y)$ is the covariance of two sets of data, x and y ; and σ_x is the standard deviation of the set x (Spearman, 1904). Here, x and y are the sub-sets of $A(t)$ and $P_c(t, z)$ defined by T . Applying equations 4 & 5 to the entire time-series forms a matrix, $R_{\Delta t}(t, z)$. A detailed justification of this range of time-scales is provided in Section 4.3. Two additional post-processing procedures were implemented after the correlations were calculated. If a subset, T , contained less than 20 valid data points, then the correlation coefficient was labelled as not a number. For the remaining data, a significance test was performed for each correlation value to ensure that the value was significantly larger than zero ($p < 0.05$). If the calculated correlation coefficient failed the significance test, it was re-assigned a value of zero.

Once the fully quality-controlled correlation analysis had been completed, we developed a simple metric to classify the mixing state of the atmospheric layer below the lowest observed cloud. First, the average below-cloud correlation coefficient, $\overline{r_{bc}}$, was calculated. When $\overline{r_{bc}} > 0$ ($p < 0.05$), the below-cloud layer was classified: “well-mixed”. In such cases, particles observed at sea-level were considered to be well-mixed into the overlying cloud. However, if the average below-cloud correlation coefficient didn’t exceed zero, then the surface layer below-cloud layer was classified: “poorly-mixed”. In these cases, the atmospheric layer at the surface was assumed to be decoupled from the overlying cloud. Finally, if there were insufficient data points in any sub-set of the time series, T , then the correlation analysis was unable to classify the mixing state of the below-cloud layer for that period.

3.2 Validation

To validate the proposed methodology and classification metric, we compared results to four separate methods of determining the mixing state of the below-cloud layer. The first two methods were variations on a conventional radiosonde analysis, one was a surface-based method and the final method was a model-based method.

We compared the classification of the below-cloud mixing state according to the correlation metric to two methods for detecting boundary layer decoupling based on radiosonde profiles. The first method searched for maxima in the virtual potential temperature gradient ($\partial\theta_v / \partial z^{-1}$) (Hande et al., 2012b). If a local maxima in the virtual potential temperature gradient was detected and found to exceed 10 K km^{-1} , then the height at which this occurred was labelled as the main inversion, or the boundary layer height. The method then searched for secondary maxima larger than 5 K km^{-1} below the main inversion. If secondary inversions exist, then the boundary layer is decoupled (Hande et al., 2012b). To be consistent with our methodology, which can only classify the atmospheric layer below the lowest observed cloud, the below-cloud layer was only labelled as decoupled if a secondary inversion was located between the surface and the cloud.

A second method for detecting below-cloud decoupling was adapted from Truong et al. (2020). In this method, a main inversion was only identified if a local

maximum in the virtual potential temperature gradient exceeded 14 K km^{-1} . To detect decoupling, the decoupling parameter μ was studied (Truong et al., 2020; Yin & Albrecht, 2000). The decoupling parameter, μ , is defined as follows:

$$\mu = - \left(\frac{\partial \theta}{\partial z} - \frac{0.608 \theta}{1 + 0.608 r} \frac{\partial r}{\partial z} \right) \quad (6)$$

Where r is the water vapour mixing ratio and θ is the potential temperature. Yin and Albrecht (2000) devised μ for their study of “transition layers” in the boundary layer, as it is more sensitive to changes in the water vapour mixing ratio than the vertical gradient of virtual potential temperature and is therefore more likely to detect subtle boundary layer features like decoupling. Decoupling of the boundary layer over the Southern Ocean was only detected when a value of μ exceeded 2.5 times its average value throughout the boundary layer (Truong et al., 2020). To be consistent with our method, we adapted this method to only classify the below-cloud layer as decoupled if the threshold for μ was exceeded in the below-cloud layer (Truong et al., 2020). We used a simple optimization methodology to determine which combination of time-scale, Δt , and correlation threshold, r_t , best predicted the state of coupling between the surface and cloud layers as compared to the reference methods (Hande et al., 2012b; Truong et al., 2020).

To provide a benchmark for our methodology, we compared the optimized performance of the correlation-based method against another surface-based methodology for defining the mixing state of the below-cloud layer (Jones et al., 2011). Briefly, if the difference in height between the observed cloud base height (CBH) and lifted condensation level (LCL) exceeded 150 m, then the below-cloud layer was considered to be decoupled from the cloud (and well-mixed otherwise). For these calculations, the LCL was calculated from the AWS measurements, where the LCL represents the height at which a cloud is expected to form based on a parcel of air adiabatically ascending through a well-mixed boundary layer (Romps, 2017). Here, we used the 1-hour averaged LCL and for consistency, the 10th-percentile of CBH within each hour.

While the radiosonde profiles collected throughout the voyage provided a robust benchmark for the new methodology, radiosonde data were available at most twice-a-day. To increase our confidence in the methodology, we compared its classification of the below-cloud layer to near-surface measures of atmospheric stability. We used two measures of near-surface atmospheric stability: the square of the Brunt-Väisälä Frequency, N^2 , and the 10-m wind speed. Values of N^2 were calculated from the AWS measurements and the COARE 3.5 bulk-flux algorithms:

$$N^2 = \frac{g}{\theta_v} \frac{\partial \theta_v}{\partial z} \quad (7)$$

where g is the gravitational acceleration, θ_v is the virtual potential temperature, and z the height above sea level. This stability analysis was combined with forecasts from AMPS to quantitatively define conditions in which aerosol–cloud coupling was expected. As a coarse proxy for aerosol-cloud coupling, we investigated the difference in the LCL and the predicted planetary boundary layer height (PBL) in the AMPS forecasts. If the planetary boundary layer exceeded the lifted condensation level, then aerosol particles measured at the ocean surface were considered well-mixed to the minimum height where cloud could have occurred.

4 Results

4.1 Time Series Analysis

Throughout the voyage to and from the Ross Sea (voyage track shown in Fig. 1a), the number–size distribution of particulate was predominantly trimodal as

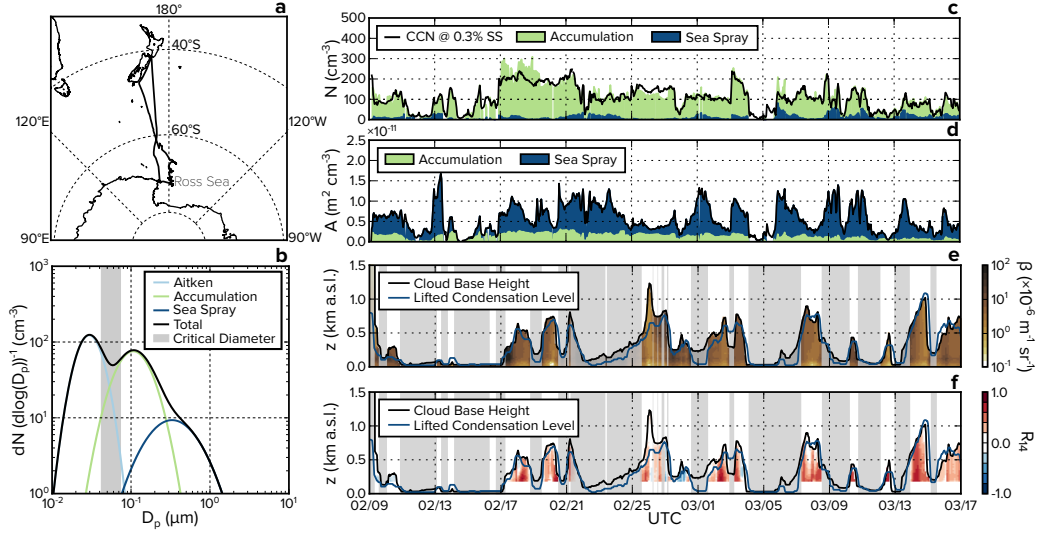


Figure 1. (a) The track of the R/V *Tangaroa* during the Marine Environment and Ecosystem Voyage. (b) A typical size distribution for particles in the Southern Ocean. The expected range of cloud activation diameters for marine stratus is shown in grey. (c) The sea-level abundance of sea spray particles (SSPs; blue filled region) and accumulation mode particles (green filled region) is compared to the abundance of cloud condensation nuclei (CCN) at a supersaturation of 0.3% (black line). (d) The abundance of suspended surface area was calculated from the measured particle size distributions (Eq. 1). (e) A contour plot of the attenuated backscatter coefficient measured by the CHM-15K ceilometer. The lifted condensation level (z_{LCL}) and cloud base height (z_{CBH}) are also shown for reference. (f) Spearman Rank correlation coefficients between the sea-level abundance of particulate surface area and ceilometer backscatter are shown. Time periods when the ceilometer optical window was obscured, the cloud base was below 200 m, fog was present, or the aerosol sampling system was contaminated by ship exhaust are shaded.

seen in Fig. 1b. The representative number–size distribution shown in Fig. 1b was constructed by taking voyage wide averages of the total number, width and median size of the individual modes that were fit to the observations. The appearance of these modes is consistent with previous observations in marine settings (Bates et al., 1998; Quinn et al., 2017). A large majority of the particles in the smallest two modes, the Aitken (30 nm, $\sigma = 1.4$) and accumulation modes (100 nm, $\sigma = 1.6$), are thought to be produced as a single mode from homogeneous nucleation of volatile sulfate species, with mode separation occurring as a result of cloud-processing (Hoppel et al., 1986). These particles are nucleated in-situ from the condensation of oxidized marine gasses and grow via self-coagulation and condensation. In contrast, sea spray particles (400 nm, $\sigma = 2$) are directly generated from breaking ocean waves, and tend to be much larger than particles in the Aitken and accumulation mode (Prather et al., 2013). Note that size statistics presented in this section have been corrected to a relative humidity of 80%. For sulfate and sea spray particles, a particle at a relative humidity of 80% is approximately twice as large compared to when it is dry (Gerber, 1985).

A representative size distribution of particles observed in the Southern Ocean marine boundary layer at a relative humidity of 80% is shown in Fig. 1b. The bifurcation of the Aitken and accumulation modes occurs when these particles pass through non-precipitating cloud, since only the largest particles will be acti-

vated (Hoppel et al., 1986). Previous research has shown that the supersaturation of water vapour within nascent marine stratus is relatively modest ($<0.3\%$; Hegg et al. (2009)). An estimation of the activation diameter based on a supersaturation of 0.3% , and a range of particle hygroscopicity parameters is also shown in Fig. 1b. The estimation of the range of activation diameter is based on the κ -Köhler model for a range of expected hygroscopicity values (Petters & Kreidenweis, 2007). This coincides well with the local minimum between the Aitken and accumulation mode, supporting the cloud-processing hypothesis of Hoppel et al. (1986).

Fig. 1c displays the number of particles in both the accumulation and sea spray modes, as these are the only particles relevant to cloud formation. This is compared to the number concentration of CCN measured at a fixed supersaturation of 0.3% . As expected, these two measurements are highly correlated. Across the entire voyage, SSPs did not comprise a substantial fraction of CCN (14%). However, in the latter half of the voyage we encountered several low pressure systems. These cyclones were accompanied by high winds, resulting in substantial wave-breaking and subsequent SSP generation in the region. This led to an enhanced relevance of SSPs to the total CCN population (20%).

Fig. 1d shows the abundance of suspended particle surface area. Despite the relatively low abundance of SSPs by number, the total amount of particulate surface area is strongly dominated by variations in their abundance. In Fig. 1e, the time series of attenuated backscatter profiles measured by a coincident ceilometer is shown, along with rolling averages of cloud base height and the lifted condensation level. As demonstrated both empirically and theoretically, if the difference between cloud base height and lifted condensation level is less than 150 m, the below-cloud layer can be considered well-mixed (Jones et al., 2011). As a result, it is clear that there was significant coupling between the surface layer and overlying cloud for much of the time-series.

4.2 New Classification Methodology

We used the Spearman Rank correlation analysis between suspended particle surface area at sea-level (Fig. 1d) and ceilometer backscatter from particles overhead (Fig. 1e) to assess whether our measurements at the surface were representative of the below-cloud population of CCN. Fig. 1f displays strong correlations between these two quantities over time-scales of 14 hours when fog, precipitation, or contamination from ship exhaust did not inhibit the analysis. This suggests that the Southern Ocean boundary layer was consistently well-mixed throughout this measurement campaign. We note that correlation coefficients could not be calculated below 200 m, as these data typically failed the SNR analysis. While one would normally expect a large backscattered signal close to a lidar, and thus a high SNR, the returning backscatter is not well-aligned with the FOV of the receiving optics in the near-range, resulting in a low SNR. As an additional control, the significance of the calculated correlation coefficients was assessed with a two-way t-test.

4.3 Comparison to Radiosonde Analysis

To validate the correlation analysis and establish the most accurate time-scale for calculating correlation coefficients, we analyzed the 57 radiosonde profiles recorded throughout the voyage. For each radiosonde, we used two gradient methods to detect whether the surface layer was decoupled from the cloud layer (Hande et al., 2012b). Out of the 57 radiosondes, three could not be used for analysis due to faulty sensors, and 21 were launched when the cloud base height was below 200 m. In such cases, there was insufficient ceilometer data to perform the correlation analysis, as the power of the returning backscatter was on the same order of magnitude

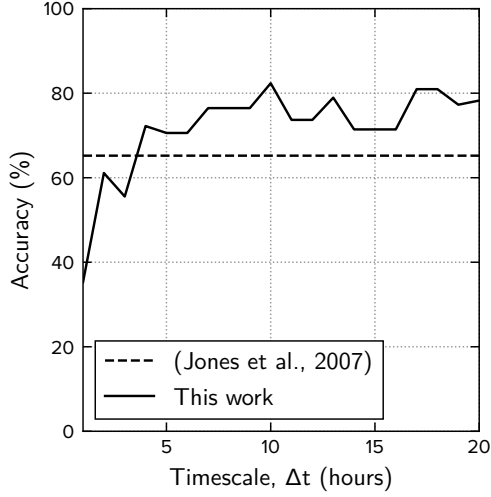


Figure 2. The accuracy with which the new correlation metric correctly classified the mixing state of the below-cloud layer for different correlation time-scales, Δt . The accuracy of the method was calculated in reference to two radiosonde analyses which classified the mixing state of the below-cloud layer based on thermodynamic gradients ($N = 26$; non-precipitating conditions, no fog, $CBH > 200$ m) (Hande et al., 2012b; Truong et al., 2020). The accuracy of the proposed method can be compared to the accuracy of another ground-based methodology of determining the state of below-cloud mixing (Jones et al., 2011).

as the instrument noise due to the FOV effects described earlier. In three additional cases, the gradient methods did not detect a boundary layer. As a result, there were only 30 radiosondes available for which the correlation analysis was valid. In these remaining 30 cases, the radiosonde-based methods of classifying the below-cloud layer differed only slightly. Overall, the below-cloud layer appeared well-mixed in 83% of profiles according to the criteria of Truong et al. (2020), and 90% of profiles according to Hande et al. (2012b).

The classifications of the below-cloud mixing state defined by the radiosonde analyses were used to define the optimal time-scale, Δt , and threshold, r_t , for the correlation analysis. For consistency, only the profiles for which both radiosonde methods agreed on the mixing state of the below-cloud layer were used as a reference when calculating the accuracy ($N = 26$). In Fig. 2, the accuracy with which the correlation analysis determined the mixing state of the below-cloud layer is shown as a function of time-scale. Across all time-scales, the threshold for detecting a well-mixed below-cloud layer was $\overline{r_{bc}} > 0$, where $\overline{r_{bc}}$ is the average correlation coefficient between sea-level and the 10th-percentile of cloud base height. As a benchmark, we have also shown the accuracy of another ground-based method for determining the below-cloud mixing state (Jones et al., 2011).

Fig. 2 demonstrates that the accuracy of the correlation-based method increased from 35% to 76% as the time-scale increased, until time-scales of 7 hours or longer were reached. Differences in accuracy at time-scales beyond 7 hours were negligible considering the sample size ($N = 26$). The increase in accuracy with increasing time-scale is a direct result of increasing the number of samples in the subset T (defined in Eq. 4) used for calculating the correlation coefficient. While shorter time-scales are likely more representative of the time-scale of turbulence,

Table 1. This table summarizes statistics comparing measurements from radiosondes launched throughout the voyage and predictions from AMPS below 3 km (a.s.l.).

Statistic	P (hPa)	T (K)	T_d (K)	U (m s^{-1})
RMSD	2.0	1.2	3.2	2.7
Bias	0.3	–	-0.8	0.7
R^2	1	0.96	0.87	0.74

RMSD: Root Mean Squared Deviation
 R^2 : Pearson Correlation Coefficient

there is also a higher likelihood that the remaining noise in the ceilometer observations will result in weaker correlations which fail the two-way t-test ($p > 0.05$). Increasing the time-scale resulted in more consistent correlation coefficients across time-scales and more statistically significant results overall. The accuracy of this method also suggests that despite there being longer time-scale phenomena which could also correlate particulate surface area and backscatter (e.g. frontal systems, convective forcing at cloud top, precipitation, turbulent perturbations of relative humidity, air mass history, etc.), these phenomena are not likely to result in substantial misclassification of the below-cloud layer. However, considering that such long time-scale phenomena do exist and may be more prevalent in other regions or observation periods, correlation coefficients calculated over time-scales beyond those presented here should be avoided as false positives and false negatives are likely to become more abundant.

Finally, we compared the accuracy of our new methodology to another method of remotely classifying the below-cloud mixing state (Jones et al., 2011). In this case, the referenced method was only 65% accurate at determining the mixing state of the below-cloud layer, whereas the proposed method was 76% accurate when correlation time-scales greater than 7 hours were considered. While the set of radiosondes for which we could compare both methods was quite limited ($N = 26$), these results suggest that the proposed method more accurately classified the mixing state of the below-cloud layer than the referenced method ($p < 0.05$).

Overall, the correlation analysis found that the below-cloud layer was well-mixed for 14% of the entire time series and poorly-mixed just 5%. Fog was found to occur 7% of the time, where fog was diagnosed when the relative humidity was measured to be 100% and cloud base was less than 50 m. The remaining portion of the time series could not be analyzed (74%), as one or more of the following occurred: the ceilometer’s quality control flag was raised; the ship exhaust contaminated the aerosol sample; or, the cloud base was below 200 m but greater than 50 m, such that the entire profile of below-cloud backscatter failed the SNR analysis due to a lack of overlap between the FOV of the ceilometer’s optical system and the returning backscatter. While this may seem like a large loss of the time-series, if a given radiosonde was only representative of conditions for the hour of measurements in which it was operating, then the radiosonde analysis provided data for just 7% of the time series. With the proposed correlation analysis, we were able to classify the boundary layer for 26% of the time series, a marked improvement.

4.4 Comparison to Stability Analysis

While the comparison to conventional radiosonde analyses provided evidence that the correlation analysis accurately classified the below-cloud mixing state, it still seemed prudent to evaluate the analysis against other metrics of atmospheric

mixing. Here, we examine expected rates of occurrence for aerosol-cloud coupling based on AMPS forecasts for the period of study.

First, the forecasts were compared to our observations from all available radiosondes, except those with non-functioning RH sensors. Table 1 provides a summary of various comparison statistics between forecasts and measurements. The statistics were only calculated below 3 km to restrict the comparison to relevant planetary boundary layer (PBL) and lifted condensation level (LCL) heights. These are presented in Table 1.

Overall, observed and measured values of the selected variables were reasonably well correlated. However, there were minor biases worth mentioning. In Table 1, statistically significant biases between modelled and measured values of pressure, dew point temperature, and wind speed were observed ($p < 0.001$). Within AMPS, the height of the PBL is determined according to the turbulent kinetic energy profile (Janjic, 2001). This implies that the height of the PBL may have been under-estimated by AMPS. The dew point temperature was also negatively biased as a result of the over-abundance of water vapour in the AMPS boundary layer relative to observations. This implies that the LCL was also under-predicted. Still, considering the spatial and temporal scale of the AMPS forecasts, the agreement between model and measured values was quite good, and highly statistically significant ($p < 0.001$).

In Fig. 3a, the frequency of occurrence with which the depth of the planetary boundary layer exceeded the lifted condensation level is shown, based on forecasts from AMPS between 40 – 70 S (excluding areas less than 100 km from a coast). The frequency of occurrence is shown as a function of two variables which are often used to describe the stability of the near-surface atmospheric layer: the square of the Brunt-Väisälä frequency, N^2 , and the 10-m wind speed, U_{10} . The results in Fig. 3a demonstrate that in near-neutral stability ($N^2 \sim 0$) and weak winds ($U_{10} \sim 0$), the layer below the LCL was less-likely to be well-mixed, as the PBL was too shallow. However, in all other cases, the boundary layer was likely well-mixed as the PBL exceeded the LCL. Note that there was still a small percentage of the time when the layer below the LCL was well-mixed despite the surface layer being near-neutrally stable. While a well-mixed boundary layer would not be expected in such cases, the near-surface layer is typically much shallower than the LCL, and is therefore not always a perfect determinant of the mixing state of the entire layer below the LCL. However, it is clear from Fig. 3a that in most other conditions, the layer below the LCL is almost guaranteed to be well-mixed. Overall, The AMPS analysis in Fig. 3a provides a general rule of thumb: if the 10 m wind speed exceeds 8 m s^{-1} then the boundary layer will be well-mixed to the LCL, regardless of the near-surface stability.

In Fig. 3c and d, the classification of the below-cloud layer according to the correlation metric is shown for time-scales of 7 and 14 hours, respectively. We can see that despite the accuracy with which the correlation analysis at 7 hour and 14 hour time-scales classified the mixing state of the boundary layer (Fig. 2), the correlation metric calculated over a 14 hour time-scale provided a more qualitatively consistent result with the AMPS analysis. In comparing Figs. 3c & d, it is clear that the correlation metric calculated over a time-scale of 7 hours misclassified the boundary layer more frequently, as a poorly mixed boundary layer is not expected to occur at all if $N^2 < -5 \times 10^{-3} \text{ s}^{-2}$ or $U_{10} > 8 \text{ m s}^{-1}$ (Fig. 3a). Barring a few exceptions, Fig. 3d shows that the correlation metric at a time-scale of 14 hours typically only classified the below-cloud layer as decoupled only when the stability of the near-surface layer was near-neutral and winds were less than 8 m s^{-1} , consistent with the AMPS analysis. While only two time-scales are presented here, analysis at all time-scales longer than 14 hours produced qualitatively similar results. Finally, in

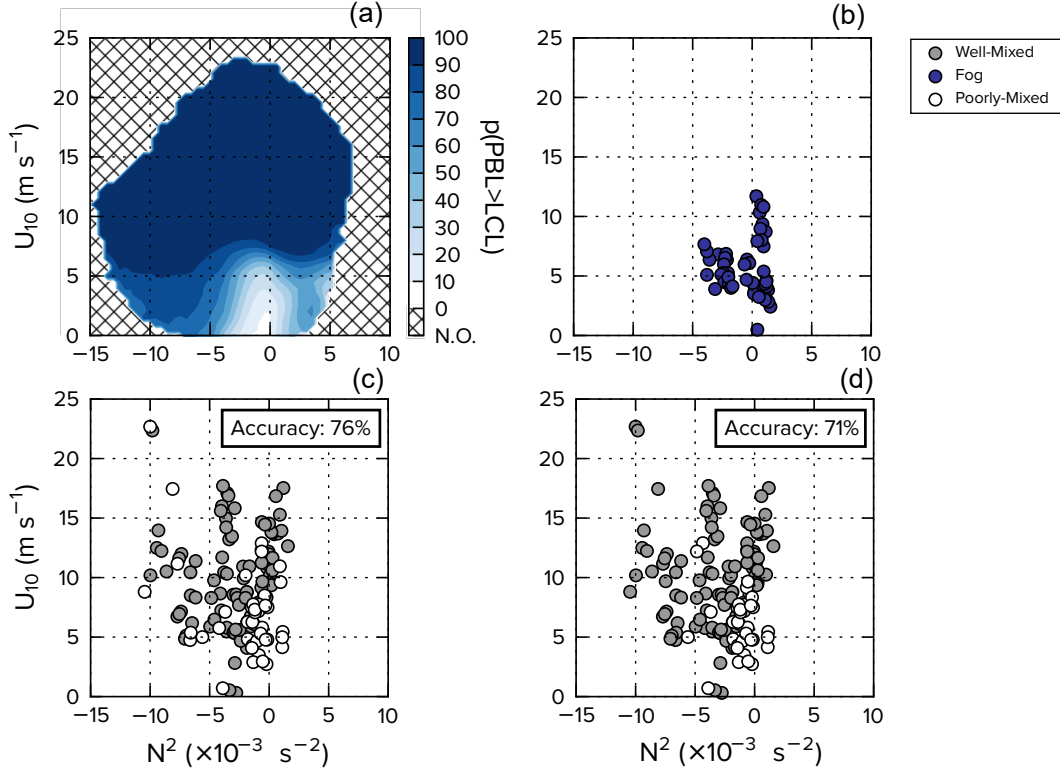


Figure 3. (a) The frequency with which the height of the planetary boundary layer (PBL) predicted by AMPS was higher than the lifted condensation level (LCL) over the open Southern Ocean (40–70 S, >100 km from coastline) in February and March 2018 (N.O. = Conditions occurred less than frequently than 0.001%). (b) The occurrence of fog (CBH < 50 m, RH = 100%). (c) The classification of the below-cloud layer based on correlation coefficients calculated over 7-hour timescales (non-precipitating conditions; CBH > 200 m). The measure of accuracy is in reference to the radiosonde analyses (Fig. 2). (d) As in (c), but for a time-scale of 14-hours.

Fig. 3b, it is clear that fog tended to occur only in both near-neutral stability ($N^2 > -5 \times 10^{-3} \text{ s}^{-2}$) and low winds, or stable conditions, consistent with advection fog.

One limitation of this analysis is that a cloud is not necessarily guaranteed to occur at the LCL. As such, a direct quantitative comparison between Figs. 3a, c & d is not possible, as cloud was always occurring in the subset of data we were able to analyze but may not have been occurring in the AMPS forecasts. Still, we found this figure to be a useful qualitative reference for our methodology. In addition, it demonstrates that even though the fraction of the time-series available for analysis via the correlation metric is low (26%; ~10 days of observations), the conditions encountered within this subset of the data are representative of the wide set of conditions forecast by AMPS. As a result, statistics presented in the previous section can be used to conclude that in non-precipitating conditions, the below-cloud layer over the Ross Sea was likely well-mixed 54% of the time, poorly-mixed 19% of the time, and contained fog 27% of the time.

5 Discussion

In this work, we were interested in understanding how often aerosol particles measured near the surface of the ocean were relevant to low cloud formation over the Southern Ocean. We proposed a new methodology, based on the correlation of particle surface area and ceilometer backscatter, which identified when aerosol particles observed at the surface were available to the lowest observed cloud. To validate the proposed methodology, we needed an accurate reference classification of the boundary layer against which we could compare our results. Here, we modified two radiosonde-based methodologies which determined the mixing state of the entire boundary layer based on gradients of thermodynamic variables (Hande et al., 2012b; Truong et al., 2020). Radiosonde-based methodologies were selected as the preferred reference methodology, as the observations were sensitive to fine thermodynamic changes in the boundary layer. These reference methodologies were modified to simply determine the mixing state of the atmosphere between the surface and the base of the lowest observed cloud. This allowed us to optimize the parameters of our proposed methodology (correlation time-scale, threshold of correlation strength) such that the predicted mixing state of the below-cloud layer best matched the referenced radiosonde methodologies. In the comparison (Fig. 2), the proposed correlation-based method correctly classified the mixing state of the below-cloud layer $76 \pm 4\%$ of the time for correlation time-scales greater than 7 hours. The accuracy of our method was then compared to a more simple metric for classifying the mixing state of the below cloud layer, which was only accurate 65% of the time (Jones et al., 2011).

In a more qualitative comparison (Fig. 3), the classification of the below-cloud mixing state by the proposed methodology was also shown to be consistent with surface-based measurements of atmospheric stability and model predictions of turbulence in a wide range of conditions. The high accuracy of the new methodology's predictions in comparison to radiosonde-based methods, in situ observations of near-surface atmospheric stability, and model forecasts of boundary layer turbulence gives us high confidence that the proposed method is accurate even when reference data is not available.

With the accuracy of our proposed methodology validated against multiple methods of determining the below-cloud mixing state, we can compare statistics to previous observations in the Southern Ocean. We find that while the below-cloud layer was often well-mixed, this was not always guaranteed. It is well-known that the marine boundary layer can stratify into a near-surface boundary layer and a sub-cloud layer (Garratt, 1994). In fact, radiosondes launched from Macquarie Island (54.62°S, 158.85°E) over the past two decades found that the boundary layer was well-mixed just 17.8% of the time (Hande et al., 2012b). In contrast, our time series analysis showed that in non-precipitating conditions, the below-cloud layer was well-mixed 54% of the time. This seems to be in stark contrast to the accuracy data presented in Fig. 2. However, the difference in frequency of occurrence comes primarily from a difference in the definition of decoupling. The method presented in this work was only designed to detect whether the boundary layer was well-mixed up to the lowest cloud. In contrast, the method used to analyze radiosondes launched from Macquarie Island was designed to detect decoupling throughout the entire boundary layer (Hande et al., 2012b). However, multi-layer clouds are frequently observed over the Southern Ocean (Hande et al., 2012b). In such settings, the inversion atop the lowest cloud will tend to decouple the atmospheric layer beneath the cloud from the rest of the boundary layer. Despite this decoupling, near-surface air is typically still well-mixed up to the lowest cloud, as cloud was often present in the atmospheric layer beneath the decoupling height (Hande et al., 2012b). As a result of this inconsistency, statistics retrieved from the radiosonde analysis at Macquarie

Island cannot be easily used to infer information about aerosol–cloud coupling and are not directly comparable to this study.

Overall, the results from the correlation analysis highlight that particles are almost always available to the lowest cloud (Fig. 1f). The percentage of time in which aerosol–cloud coupling occurred within the valid section of our time series is simply the sum total of the rates of occurrence of fog and a well-mixed below-cloud layer: 81%. Forecasts from AMPS tend to agree, as the layer of the atmosphere below the LCL was found to be well-mixed 84% of the time over the Southern Ocean throughout February and March 2018. Based on the good agreement between these methods of defining the below-cloud mixing state, we are confident in concluding that sea spray particles are available to low-level cloud over the Southern Ocean more than 80% of the time in austral summer. As Kuma et al. (2020) noted, the ability to correctly predict the occurrence of low cloud is a critical necessity for improving the Southern Ocean shortwave radiation bias. The proposed method increases our understanding of these low clouds and the particles which help form them.

For instance, we found that the number of CCN at a supersaturation of 0.3% was consistent with the number of particles in the accumulation and sea spray mode. As a supersaturation of 0.3% is the expected water vapor supersaturation within marine stratocumulus (Hegg et al., 2009), this suggests that sea-level observations may provide a good constraint on the number of cloud droplets in a wide variety of conditions. We found that despite being readily-available to nascent clouds, sea spray particles were typically outnumbered by smaller, cloud-processed accumulation mode particles (Fig. 1c), consistent with previous studies (Quinn et al., 2017). However, in addition to abundance, the ice-nucleating ability of particles is known to be a strong determinant of cloud phase and albedo: a climate model which determined the primary nucleation of ice within low-level clouds according to the abundance and type of boundary layer ice-nucleating particles found that predictions of cloud opacity were significantly more accurate in the cold sector of Southern Ocean cyclones relative to simpler glaciation schemes (Vergara-Temprado et al., 2018). Though less numerous than accumulation mode particles, sea spray particles are thought to be the only local source of ice-nucleating particles (DeMott et al., 2016) in a region that is often devoid of more potent ice nuclei (e.g. dust) (McCluskey et al., 2018). This study highlights that sea spray particles are available to many more cloud systems than just within the cold sector of cyclones. As a result, climate models which implement glaciation schemes that connect the primary nucleation of ice to the microphysical properties of aerosol particles will likely see more widespread improvement to the Southern Ocean shortwave radiation bias. It also highlights that should models adopt more complex models of cloud glaciation, then they must also more carefully parameterize the flux of sea spray particles (Hartery et al., 2020).

The new method does not come without limitations, however. Depending on the FOV of the ceilometer’s optical receiver, the ability of the analysis to analyze below-cloud coupling in low cloud settings ($CBH < 200$ m) can be severely impaired due to an incomplete overlap of the returning laser beam and the receiver’s FOV. In addition, though we have provided a reasonably comprehensive validation of the appropriate time-scale for calculating correlation coefficients and the threshold for classification of the below-cloud layer, there are potentially instances where the correlation analysis could trigger false positives and false negatives in other synoptic settings. These include, but are not limited to, frontal systems, convective forcing at cloud top, precipitation, turbulent perturbations of relative humidity, air mass history, etc. Still, given the accuracy of the methodology as quantitatively compared to the radiosonde analyses, and qualitatively to a forecast analysis, we are confident in the results presented as they pertain to this specific region and period of study. As an added benefit, the proposed method also uses instruments which function

nearly autonomously, with little need for oversight or on-site personnel. In contrast, radiosonde programs require highly-trained personnel and can only be launched in a limited set of meteorological conditions. It becomes exceedingly difficult to successfully launch a radiosonde once winds surpass 15 m s^{-1} , and potentially dangerous when aboard a research vessel in unfavorable wave conditions. As a result, statistics of boundary layer mixing collected from radiosonde programs are likely skewed towards calm conditions. Finally, it is worth mentioning that there are likely unintended, negative environmental consequences of leaving irretrievable radiosonde packages in the Southern Ocean.

6 Conclusions

In this work we presented a new technique for determining the state of boundary layer mixing based on the value of the Spearman Rank correlation coefficient calculated between sea-level observations of suspended particle surface area and ceilometer backscatter. When data was available, these correlations were often high, implying that particles measured at sea-level were well-mixed throughout the boundary layer and were therefore readily-available to nascent, low-level cloud. From this analysis, a simple metric was created to diagnose whether coupling occurred or not. This revealed that in non-precipitating conditions the boundary layer was well-mixed 54% of the time, contained fog 27% of the time, and was poorly-mixed just 19% of the time. This simple metric based on the correlation analysis was compared to two conventional radiosonde analyses. The correlation-based metric accurately classified the mixing state of the boundary layer 76% of the time when correlation coefficients were calculated over periods longer than 7 hours. This is a noticeable improvement over the accuracy of a simpler ground-based method (65%). In addition, the frequency of occurrence of below-cloud mixing estimated by the correlation-based metric was qualitatively consistent with an analysis of mixing based on the near-surface stability within regional forecasts. We estimate that aerosol will have a direct pathway into low cloud either through a well-mixed below cloud layer or surface-level fog, 81% of the time when clouds are present. Thus, in situ sea-level observations of particulate offer substantial insight into cloud formation over the Southern Ocean in a wide set of conditions.

Acknowledgments

This project was funded through the New Zealand Deep South National Science Challenge Cloud and Aerosols project (2017–19). The Antarctic voyage operations were supported through a New Zealand Crown Funding Agreement and associated voyage science was funded through the National Institute of Water and Atmospheric Research’s Research Programme in Ocean-Climate Interactions (2017/19 SCI). S.H. acknowledges support from the University of Canterbury Doctoral Scholarship. The authors would like to acknowledge R/V *Tangaroa* Captain Evan Solly, fellow officers and associated crew for safe passage throughout the voyage in addition to the fellow sea-going scientific staff and voyage leader Dr David Bowden. Additional thanks to Simon Parsons and Graeme Plank for the installation of the ceilometer on the R/V *Tangaroa* and logistical support of the radiosonde programme. Observational data from the R/V *Tangaroa* used in this study are available for download at: https://zenodo.org/record/4060237#.X_xcK-hKiMo. AMPS data used in this study were downloaded from: <https://www.earthsystemgrid.org/project/amps.html>.

References

Bates, T. S., Huebert, B. J., Gras, J. L., Griffiths, F. B., & Durkee, P. A. (1998).

- International global atmospheric chemistry (igac) project's first aerosol characterization experiment (ace 1): Overview. *Journal of Geophysical Research: Atmospheres*, 103(D13), 16297–16318.
- Bigg, E. K., & Hopwood, S. C. (1963). Ice nuclei in the antarctic. *Journal of the Atmospheric Sciences*, 20(3), 185–188. doi: 10.1175/1520-0469(1963)020<0185:INITA>2.0.CO;2
- Bodas-Salcedo, A., Williams, K. D., Ringer, M. A., Beau, I., Cole, J. N., Dufresne, J.-L., ... Yokohata, T. (2014). Origins of the solar radiation biases over the Southern Ocean in CFMIP2 models. *Journal of Climate*, 27(1), 41–56.
- Boers, R., Jensen, J., & Krummel, P. (1998). Microphysical and short-wave radiative structure of stratocumulus clouds over the southern ocean: Summer results and seasonal differences. *Quarterly Journal of the Royal Meteorological Society*, 124(545), 151–168.
- Bohren, C. F., & Huffman, D. R. (1983). Absorption and scattering by a sphere. *Absorption and scattering of light by small particles*.
- Borys, R. D., Lowenthal, D. H., Cohn, S. A., & Brown, W. O. J. (2003). Mountaintop and radar measurements of anthropogenic aerosol effects on snow growth and snowfall rate. *Geophysical Research Letters*, 30(10). doi: 10.1029/2002GL016855
- DeMott, P. J., Hill, T. C. J., McCluskey, C. S., Prather, K. A., Collins, D. B., Sullivan, R. C., ... Franc, G. D. (2016). Sea spray aerosol as a unique source of ice nucleating particles. *Proceedings of the National Academy of Sciences*, 113(21), 5797–5803. doi: 10.1073/pnas.1514034112
- Edson, J. B., Jampana, V., Weller, R. A., Bigorre, S. P., Plueddemann, A. J., Fairall, C. W., ... Hersbach, H. (2013). On the exchange of momentum over the open ocean. *Journal of Physical Oceanography*, 43(8), 1589–1610. doi: 10.1175/JPO-D-12-0173.1
- Garratt, J. (1994). Review: the atmospheric boundary layer. *Earth-Science Reviews*, 37(1), 89 - 134. Retrieved from <http://www.sciencedirect.com/science/article/pii/0012825294900264> doi: [https://doi.org/10.1016/0012-8252\(94\)90026-4](https://doi.org/10.1016/0012-8252(94)90026-4)
- Gerber, H. E. (1985). *Relative-humidity parameterization of the Navy Aerosol Model (NAM)* (Tech. Rep.). Washington, DC: Naval Research Lab.
- Hande, L., Siems, S., & Manton, M. (2012a). Observed trends in wind speed over the Southern Ocean. *Geophysical Research Letters*, 39(11). doi: 10.1029/2012GL051734
- Hande, L., Siems, S., Manton, M., & Belusic, D. (2012b). Observations of wind shear over the southern ocean. *Journal of Geophysical Research: Atmospheres*, 117(D12). doi: 10.1029/2012JD017488
- Hande, L. B., Siems, S. T., Manton, M. J., & Lenschow, D. H. (2015). An evaluation of cosmic radio occultation data in the lower atmosphere over the southern ocean. *Atmospheric Measurement Techniques*, 8(1), 97–107. Retrieved from <https://amt.copernicus.org/articles/8/97/2015/> doi: 10.5194/amt-8-97-2015
- Hartery, S., Toohey, D., Revell, L., Sellegri, K., Kuma, P., Harvey, M., & McDonald, A. (2020). Constraining the surface flux of sea spray particles from the southern ocean. *Journal of Geophysical Research: Atmospheres*, 125(4). doi: 10.1029/2019JD032026
- Haynes, J. M., Jakob, C., Rossow, W. B., Tselioudis, G., & Brown, J. (2011). Major characteristics of southern ocean cloud regimes and their effects on the energy budget. *Journal of Climate*, 24(19), 5061–5080. doi: 10.1175/2011JCLI4052.1
- Hegg, D. A., Covert, D. S., Jonsson, H. H., & Woods, R. (2009). Differentiating natural and anthropogenic cloud condensation nuclei in the california coastal zone. *Tellus B: Chemical and Physical Meteorology*, 61(4), 669–676. doi: 10.1111/j.1600-0889.2009.00435.x

- Hoppel, W. A., Frick, G. M., & Larson, R. E. (1986). Effect of nonprecipitating clouds on the aerosol size distribution in the marine boundary layer. *Geophysical Research Letters*, 13(2), 125-128. doi: 10.1029/GL013i002p00125
- Hu, Y., Rodier, S., Xu, K.-M., Sun, W., Huang, J., Lin, B., ... Josset, D. (2010). Occurrence, liquid water content, and fraction of supercooled water clouds from combined caliop/iir/modis measurements. *Journal of Geophysical Research: Atmospheres*, 115(D4).
- Irving, D., Simmonds, I., & Keay, K. (2010). Mesoscale cyclone activity over the ice-free southern ocean: 1999–2008. *Journal of Climate*, 23(20), 5404-5420. doi: 10.1175/2010JCLI3628.1
- Janjic, Z. I. (2001). *Nonsingular implementation of the mellor-yamada level 2.5 scheme in the ncep meso model* (Office Note No. 437). National Center for Environmental Prediction (NCEP).
- Jolly, B., McDonald, A. J., Coggins, J. H. J., Zawar-Reza, P., Cassano, J., Lazara, M., ... Dale, E. (2016). A validation of the Antarctic mesoscale prediction system using self-organizing maps and high-density observations from SNOWWEB. *Monthly Weather Review*, 144(9), 3181-3200. doi: 10.1175/MWR-D-15-0447.1
- Jones, C. R., Bretherton, C. S., & Leon, D. (2011). Coupled vs. decoupled boundary layers in vocals-rex. *Atmospheric Chemistry and Physics*, 11(14), 7143–7153. Retrieved from <https://acp.copernicus.org/articles/11/7143/2011/> doi: 10.5194/acp-11-7143-2011
- Korhonen, H., Carslaw, K. S., Forster, P. M., Mikkonen, S., Gordon, N. D., & Kokkola, H. (2010). Aerosol climate feedback due to decadal increases in southern hemisphere wind speeds. *Geophysical Research Letters*, 37(2). doi: 10.1029/2009GL041320
- Kremser, S., Harvey, M., Kuma, P., Hartery, S., Saint-Macary, A., McGregor, J., ... Parsons, S. (2020). Southern ocean cloud and aerosol data: a compilation of measurements from the 2018 southern ocean ross sea marine ecosystems and environment voyage. *Earth System Science Data*(submitted).
- Kuma, P., McDonald, A. J., Morgenstern, O., Alexander, S. P., Cassano, J. J., Garrett, S., ... Williams, J. (2020). Evaluation of southern ocean cloud in the hadgem3 general circulation model and merra-2 reanalysis using ship-based observations. *Atmospheric Chemistry and Physics*, 20(11), 6607–6630. doi: 10.5194/acp-20-6607-2020
- McCluskey, C. S., Hill, T. C. J., Humphries, R. S., Rauker, A. M., Moreau, S., Strutton, P. G., ... DeMott, P. J. (2018). Observations of ice nucleating particles over Southern Ocean waters. *Geophysical Research Letters*, 45(21), 11,989-11,997. doi: 10.1029/2018GL079981
- McCoy, D. T., Burrows, S. M., Wood, R., Grosvenor, D. P., Elliott, S. M., Ma, P.-L., ... Hartmann, D. L. (2015). Natural aerosols explain seasonal and spatial patterns of Southern Ocean cloud albedo. *Science Advances*, 1(6). doi: 10.1126/sciadv.1500157
- McErlich, C., McDonald, A., Schuddeboom, A., & Silber, I. (2021). Comparing satellite- and ground-based observations of cloud occurrence over high southern latitudes. *Journal of Geophysical Research: Atmospheres*, 126(6). doi: <https://doi.org/10.1029/2020JD033607>
- McFarquhar, G. M., Bretherton, C., Marchand, R., Protat, A., DeMott, P. J., Alexander, S. P., ... McDonald, A. (2020). Observations of clouds, aerosols, precipitation, and surface radiation over the southern ocean: An overview of capricorn, marcus, micre and socrates. *Bulletin of the American Meteorological Society*, 1 - 92. doi: 10.1175/BAMS-D-20-0132.1
- Modini, R. L., Frossard, A. A., Ahlm, L., Russell, L. M., Corrigan, C. E., Roberts, G. C., ... Leaitch, W. R. (2015). Primary marine aerosol-cloud interactions off the coast of California. *Journal of Geophysical Research: Atmospheres*, 120(9),

- 4282-4303. doi: 10.1002/2014JD022963
- Petters, M. D., & Kreidenweis, S. M. (2007). A single parameter representation of hygroscopic growth and cloud condensation nucleus activity. *Atmospheric Chemistry and Physics*, 7(8), 1961–1971. Retrieved from <http://www.atmos-chem-phys.net/7/1961/2007/> doi: 10.5194/acp-7-1961-2007
- Prather, K. A., Bertram, T. H., Grassian, V. H., Deane, G. B., Stokes, M. D., DeMott, P. J., ... Zhao, D. (2013). Bringing the ocean into the laboratory to probe the chemical complexity of sea spray aerosol. *Proceedings of the National Academy of Sciences*, 110(19), 7550–7555. doi: 10.1073/pnas.1300262110
- Pruppacher, H. R., Klett, J. D., & Wang, P. K. (1998). *Microphysics of clouds and precipitation*. Taylor & Francis.
- Quinn, P. K., Coffman, D. J., Johnson, J. E., Upchurch, L. M., & Bates, T. S. (2017). Small fraction of marine cloud condensation nuclei made up of sea spray aerosol. *Nature Geoscience*, 10, 674–679. doi: 10.1038/ngeo3003
- Romps, D. M. (2017). Exact expression for the lifting condensation level. *Journal of the Atmospheric Sciences*, 74(12), 3891–3900. doi: 10.1175/JAS-D-17-0102.1
- Russell, L. M., Lenschow, D. H., Laursen, K. K., Krummel, P. B., Siems, S. T., Bandy, A. R., ... Bates, T. S. (1998). Bidirectional mixing in an ace 1 marine boundary layer overlain by a second turbulent layer. *Journal of Geophysical Research: Atmospheres*, 103(D13), 16411–16432.
- Schuddeboom, A., Varma, V., McDonald, A. J., Morgenstern, O., Harvey, M., Parsons, S., ... Furtado, K. (2019). Cluster-based evaluation of model compensating errors: A case study of cloud radiative effect in the Southern Ocean. *Geophysical Research Letters*, 46(6), 3446–3453. doi: 10.1029/2018GL081686
- Spearman, C. (1904). The proof and measurement of association between two things. *The American Journal of Psychology*, 15(1), 72–101. Retrieved from <http://www.jstor.org/stable/1412159>
- Trenberth, K. E., & Fasullo, J. T. (2010). Simulation of present-day and twenty-first-century energy budgets of the Southern Oceans. *Journal of Climate*, 23(2), 440–454.
- Truong, S. C. H., Huang, Y., Lang, F., Messmer, M., Simmonds, I., Siems, S. T., & Manton, M. J. (2020). A climatology of the marine atmospheric boundary layer over the southern ocean from four field campaigns during 2016–2018. *Journal of Geophysical Research: Atmospheres*, 125(20), e2020JD033214. doi: <https://doi.org/10.1029/2020JD033214>
- Twomey, S. (1977). The influence of pollution on the shortwave albedo of clouds. *Journal of the Atmospheric Sciences*, 34(7), 1149–1152. doi: 10.1175/1520-0469(1977)034<1149:TIOPOT>2.0.CO;2
- Vergara-Temprado, J., Miltenberger, A. K., Furtado, K., Grosvenor, D. P., Shipway, B. J., Hill, A. A., ... Carslaw, K. S. (2018). Strong control of southern ocean cloud reflectivity by ice-nucleating particles. *Proceedings of the National Academy of Sciences*, 115(11), 2687–2692. doi: 10.1073/pnas.1721627115
- Wofsy, S. C. (2011). Hiaper pole-to-pole observations (hippo): fine-grained, global-scale measurements of climatically important atmospheric gases and aerosols. *Philosophical Transactions of the Royal Society A: Mathematical, Physical and Engineering Sciences*, 369(1943), 2073–2086. doi: 10.1098/rsta.2010.0313
- Yin, B., & Albrecht, B. A. (2000). Spatial variability of atmospheric boundary layer structure over the eastern equatorial pacific. *Journal of Climate*, 13(9), 1574–1592. doi: 10.1175/1520-0442(2000)013<1574:SVOABL>2.0.CO;2
- Young, I. R., Zieger, S., & Babanin, A. V. (2011). Global trends in wind speed and wave height. *Science*, 332(6028), 451–455. doi: 10.1126/science.1197219